

2.C Hydrodynamic Simulations of Thermal Self-Focusing in Laser-Generated Plasmas

Self-focusing of the incident laser radiation in the underdense coronal plasmas of laser-fusion targets has long been recognized as a mechanism which can enhance irradiation nonuniformities, thus disrupting the high-compression implosions of these targets. This phenomenon is understood to involve a close interaction between perturbations to the plasma density profile caused by thermal or ponderomotive pressure gradients and propagation of the laser in the perturbed plasma. Numerous experimental observations of self-focusing in underdense plasmas have been reported.¹ As laser-fusion research moves towards larger targets, producing longer density scale lengths in the underdense corona, the possibility of thermal self-focusing will become an increasingly serious consideration. For this reason, we have performed a number of simulations of this mechanism, including realistic 2-D hydrodynamics.

A distinction is generally made between thermal and ponderomotive self-focusing. In the first case, the thermal pressure associated with a laser-heated plasma causes a reduction in the plasma density and, therefore, an increase in the plasma refractive index; in the geometrical-optics approximation, incident laser rays are then refracted in such a way as to enhance the perturbation. In ponderomotive self-focusing, sometimes referred to as filamentation, it is the ponderomotive force of an intense electromagnetic wave that distorts the plasma. This latter mechanism is expected to be particularly effective for perturbations with short spatial scale lengths, typically as small as the wavelength of the incident radiation, provided that the laser intensity is sufficiently high so that the ponderomotive pressure can balance the pressure jump associated with a significant electron-density perturbation. Thermal self-focusing is expected to be less important on these scale lengths, as it is difficult to sustain a thermal pressure gradient over distances which are, in typical cases, comparable to or less than an electron mean free path. On the other hand, for larger-scale-length modulations, thermal conduction is less effective in smoothing out temperature perturbations, and we expect thermal self-focusing to be the dominant mechanism. There may be situations where self-focusing is initiated by the thermal mechanism, but subsequently develops into ponderomotive self-focusing after the beam is focused to a small diameter. Here, however, we will confine our discussion to thermal self-focusing.

Many theoretical treatments of thermal self-focusing have been reported in the literature.^{2,3} Generally, simplifying assumptions are made about the plasma behavior, although full 1-D hydrodynamic calculations have been performed.³ In actual experimental situations, the electron-density distribution and, hence, the refractive index in the plasma corona are dependent on the full time history of the hydrodynamics; and the interaction process thereby becomes considerably more complex than can be treated analytically. The electromagnetic energy propagation must be coupled self-consistently with the 2-D

plasma hydrodynamics, including the heating and ablation processes. The purpose of this article is to present a number of such calculations, covering a broad range of conditions, using the 2-D Eulerian hydrodynamics code *SAGE* which includes a self-consistent ray-tracing algorithm for energy propagation and absorption. These calculations are not limited in relevance by the use of simplified hydrodynamic models, and are therefore able to follow the full temporal evolution of the self-focusing process. In general it is whole-beam self-focusing which is modeled here, but, to the extent permitted by the resolution of the computational grid and the neglect of diffraction, small-scale self-focusing is also modeled. The price paid for a more realistic hydrodynamic treatment is a less realistic electromagnetic propagation model, since the geometrical-optics assumption implied by the use of ray tracing excludes diffractive effects; however, this is probably not a serious concern for a wide range of experiments carried out in the near field of a laser beam, particularly for the conditions of interest in this article.

On account of the wide range of initial conditions and plasma configurations that may be encountered, we will not attempt to seek specific criteria which will determine simply, in a binary sense, whether or not self-focusing occurs. It is more instructive to consider a variety of cases which illustrate the circumstances in which self-focusing is likely to develop, and demonstrate the nonlinear evolution of the process. Variables such as the laser wavelength, pulse width and spatial intensity profile, and the initial plasma density and temperature profiles, can all be important. It is possible, however, to draw some general conclusions; for example, whole-beam self-focusing is more likely to occur when the beam diameter is small (typically less than the plasma scale length), when the background plasma is cold, and when the incident laser intensity is high.

Computational Model

For the calculations reported here, the code *SAGE* has been used in 2-D cylindrical geometry (r,z). The simplest physical model needed to treat realistically the dynamics of the underdense plasma has been adopted. A perfect-gas equation of state and a one-temperature fluid are assumed; and radiation emission, suprathreshold-electron generation, and magnetic-field effects are omitted. Thermal conduction is modeled using a standard "flux-limiter" formulation,⁴ in which the heat flux q is directed antiparallel to the temperature gradient but limited in magnitude to a given fraction of the free-streaming flux. For the low-atomic-number (CH) targets considered here, most of these assumptions are well justified. Calculations with *SAGE*, including a more complete physical description, show that (1) a real equation of state is unnecessary since the corona is fully ionized; (2) use of a two-temperature model leads to results similar to those obtained from the one-temperature model since the ions have a low heat capacity compared with the electrons; and (3) radiation emission is small. Suprathreshold electrons generated at the critical density by resonance absorption are unlikely to be important for the short wavelengths and long scale lengths under consideration. On the other hand, magnetic fields could be important, particularly if steep temperature gradients

resulting from self-focusing enhance their generation, but their treatment is outside the scope of this paper. The flux-limited treatment of thermal conduction, although ad hoc, is required to provide a reasonably accurate calculation of the absorption fraction.⁵

The code *SAGE* makes use of a general, fully three-dimensional (3-D), ray-tracing model (TRACER-3) which calculates ray trajectories through arbitrary refractive-index profiles.⁶ A ray trajectory, parametrized by the path distance s , is given by $\mathbf{r}(s)$ where \mathbf{r} obeys the equation⁷

$$\frac{d}{ds} \mu \frac{d\mathbf{r}}{ds} = \nabla \mu \quad (1)$$

with μ the refractive index. For a plasma, $\mu = (1 - n_e/n_c)^{1/2}$, where n_e is the local electron density and n_c is the critical electron density corresponding to the wavelength λ of the irradiation. Equation (1) is integrated by introducing the direction-cosine vector, \mathbf{c} , and solving the coupled first-order equations

$$\frac{d}{ds} \mathbf{r} = \mathbf{c} \quad (2)$$

$$\frac{d}{ds} (\mu \mathbf{c}) = \nabla \mu \cdot \quad (3)$$

The absorption fraction is calculated from the integral of the inverse-bremsstrahlung coefficient K_{IB} along the ray path. The refractive index $\mu(s)$ is determined here by interpolation from the electron-density distribution n_e stored on the 2-D hydrodynamic grid. The limiting factor affecting the accuracy of the trajectory calculations reported here is the resolution of the grid, which limits the accuracy with which $n_e(\mathbf{r})$ and therefore $\mu(\mathbf{r})$ are known. In all of these simulations, at least 50 rays are followed each timestep for typically 1000 hydrodynamic timesteps. Almost identical results are obtained in cases where only half as many rays are used each timestep. For a given amount of computer time, better statistics are probably obtained using 50 rays each timestep rather than ~ 500 rays every ten timesteps, since small noise perturbations in ray directions are induced by small noise fluctuations in the (changing) electron-density profile.

In summary, the four main physical processes being modeled are basic hydrodynamics, thermal conduction, inverse-bremsstrahlung absorption, and refraction. All of these play important roles in determining the onset and development of thermal self-focusing in laser-produced plasmas.

Illustrative Calculation

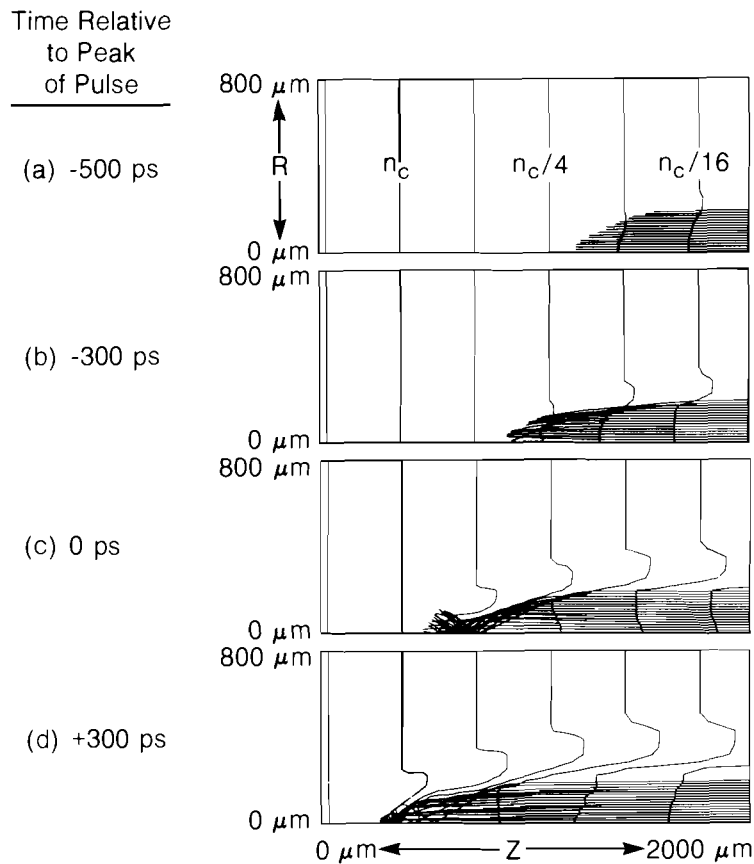
We will commence by examining a "standard" calculation, which clearly exhibits whole-beam self-focusing, before proceeding to consider some parametric variations. The laser is assumed to have a wavelength of 351 nm, Gaussian temporal and spatial profiles, a pulse length (full width at half maximum) of $t_{FW} = 600$ ps, and a nominal beam radius r_{90} (defined at the 10% intensity point or equivalently the

90% energy point) of $200 \mu\text{m}$. The peak intensity in space and time is $9 \times 10^{14} \text{ W/cm}^2$, and the nominal intensity I [defined as $J/(\pi r_{90}^2 t_{FW})$ where J is the laser energy] is $4 \times 10^{14} \text{ W/cm}^2$. The spatial profile is actually truncated at the nominal radius, the intensity being set to zero for $r > r_{90}$; this is done to avoid tracing many rays which carry little energy.

The plasma is assumed to have an initial exponential density profile of (e-folding) scale length $L = 500 \mu\text{m}$, and it is assumed to be cold (we use an initial temperature of 0.01 eV). This configuration corresponds quite closely with experiments in which a high-intensity beam interacts with a long-scale-length preformed plasma; for example, an experiment using a $1\text{-}\mu\text{m}$ wavelength but otherwise similar parameters was recently reported^{8,9} and provided some indications of self-focusing.⁹ This configuration (but with a higher background temperature) could also relate to situations where a hot spot appears in a laser beam some time into the interaction, after the plasma has developed a large scale length. One important dimensionless parameter, R , which may be thought of as the relative beam radius, is defined as the ratio of the beam radius to the plasma scale length: $R = r_{90}/L$. For the standard case, $R = 0.4$. It will become apparent that R and the other parameters have been chosen to facilitate whole-beam self-focusing.

Results are presented in Fig. 18.14, at four successive times measured relative to the peak of the pulse. Electron-density contours are drawn at the critical density n_c and at integer powers of $2 \times n_c$. The laser is incident from the right, along the target normal, with rays propagating initially parallel to the z axis. Rays are followed in the hydrodynamic calculation until all but one part in 10^5 of their energy is deposited or until they leave the simulation region. In the plotting program, however, they are terminated when 90% of their energy has been deposited. Here, and in most of the other calculations, the initial radii of the rays are distributed uniformly over $0 \leq r \leq r_{90}$, 50 rays are used per calculation cycle, and one out of every three rays is plotted. This calculation employed 60 grid points uniformly spaced in the z direction, and 24 in the r direction, variably spaced with the smallest zones near the z axis and the zone size expanding by a constant ratio from zone to zone.

Whole-beam self-focusing is observed to have occurred by the peak of the pulse [Fig. 18.14(c)]; its origin may be traced from the earlier plots [Figs. 18.14(a) and 18.14(b)]. Early in time [Fig. 18.14(a)], the laser is absorbed efficiently by the initially cold underdense plasma below quarter-critical. On the axis, where the incident intensity is the highest, the plasma is heated the most; the inverse-bremsstrahlung absorption coefficient K_B , which scales as $T_e^{-3/2}$, is therefore reduced more on-axis than off-axis, resulting in the enhanced propagation of the 90%-energy-deposition contour on-axis as seen in Fig. 18.14(a). Material is ablated from the heated region, back toward the laser and also radially outward. The radial pressure gradient is initially strong at the edge of the beam, at the discontinuity resulting from truncating the radially Gaussian intensity profile at the



TC1514

Fig. 18.14

Results at four times during the standard calculation. Time is measured relative to the peaks of the laser pulse and the laser pulse is propagating from right to left. The electron density contours are shown for the critical density n_c and at integer powers of $2 \times n_c$. The rays are terminated when 90% of their energy has been absorbed. Whole-beam self-focusing is clearly evident at the peak of the laser pulse (c).

10% intensity point. Incident rays are then refracted into this low-density region, their deflections becoming greater as they approach the critical-density surface. It will be noted that some rays pass through the axis before terminating. Removal of mass from the central (on-axis) region is enhanced by both lateral expansion in the cylindrical plasma, and by the incident energy flux becoming more intense when focused onto the axis. Self-focusing is enhanced by both of these geometrical factors.

Parametric Variations

A comparison calculation is illustrated in Fig. 18.15. Here all the parameters are unaltered, except that the beam radius has been doubled and the laser energy increased by a factor of 4 to maintain the same intensity. The four plots correspond to the same times as in Fig. 18.14. In this case no significant self-focusing occurs: no rays are bent a significant fraction of the beam radius, with the exception of a few rays at the edge of the beam in Fig. 18.15(d). Here the plasma scale length is too small in comparison with the beam radius; quantitatively, the geometrical aspect ratio (or relative beam radius)

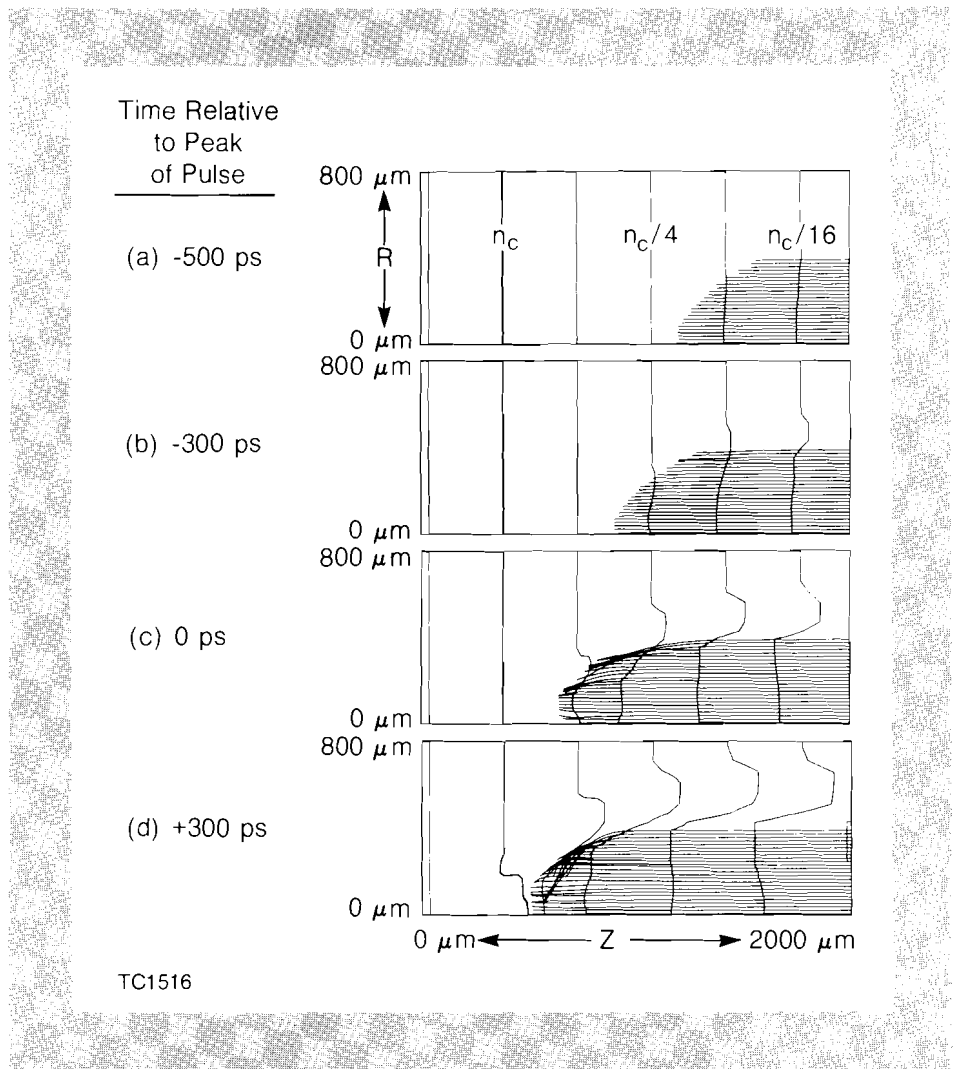


Fig. 18.15
 Results for the standard parameters, but with the beam radius doubled while maintaining the intensity. Whole-beam self-focusing is not evident at the peak of the pulse.

r_{90}/L is 0.8, compared with 0.4 in the previous (standard) case. For the irradiation parameters under consideration, a threshold for significant self-focusing occurs at a value of r_{90}/L somewhere between these two values.

It is also interesting to compare the rates of propagation of the beam into the plasma in the two cases, measured along the z axis. Initially the burn front moves at the same speed (up to 300 ps before the peak of the pulse), but when self-focusing occurs in Fig. 18.14, the front penetrates faster and deeper into the plasma.

The effect of increasing the laser intensity may be readily seen by comparing Fig. 18.16, where the intensity has been doubled, with the standard case (Fig. 18.14). The same qualitative behavior occurs, the main difference being that the beam now propagates somewhat faster and self-focusing occurs somewhat earlier. At 300 ps before the peak of the pulse, a tight beam focus appears at half-critical, but this disappears by the peak of the pulse as a result of further expulsion of plasma from the underdense heated region.

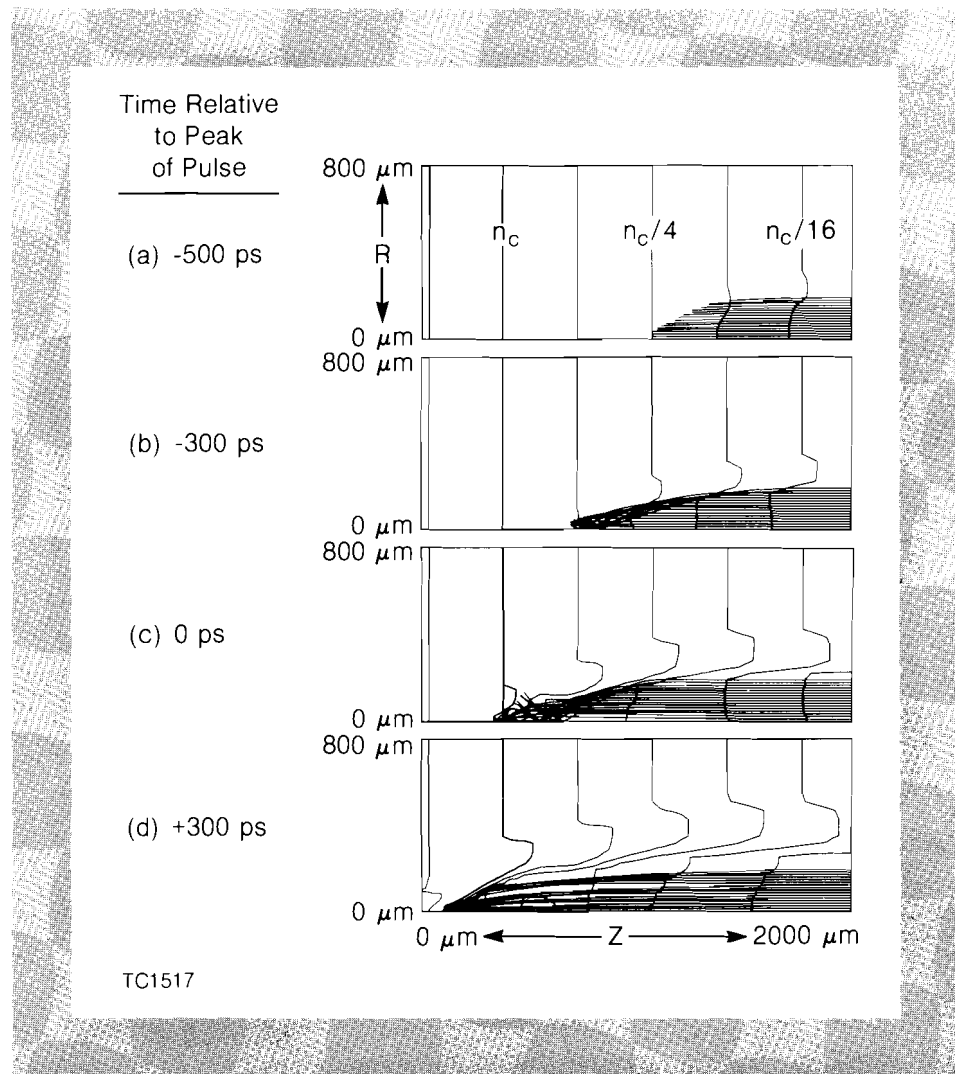


Fig. 18.16
Results for the standard parameters, but with the intensity doubled. Whole-beam self-focusing is evident as early as (b) and the propagation depth is increased due to the self-focusing.

To examine the effect of laser wavelength, the standard calculation has been repeated but with the laser wavelength increased by a factor of 3 to 1054 nm. Self-focusing also occurs in this case, as is shown in Fig. 18.17. The same initial density profile is used; thus, the critical surface appears further to the right. The laser quickly burns through the underdense plasma, reaching critical density by $t = -500$ ps [Fig. 18.17(a)]. Thereafter, whole-beam self-focusing results in a narrow conical-shaped burn front propagating into what was initially an overdense plasma. The increased complexity in Figs. 18.17(b) and 18.17(c) arises because of the reduced inverse-bremsstrahlung absorption that occurs at longer wavelengths: most rays have not suffered 90% attenuation by the time they reach the vicinity of the critical surface, and so their return trajectories are plotted.

It is interesting to note that these rays return well-collimated toward the incident laser, even though they undergo substantial angular spreading in the vicinity of critical. In this calculation approximately half of the incident laser energy is reflected, and 80% of the reflected light returns to within 12° of the laser axis (see Fig. 18.18). In the 3-D

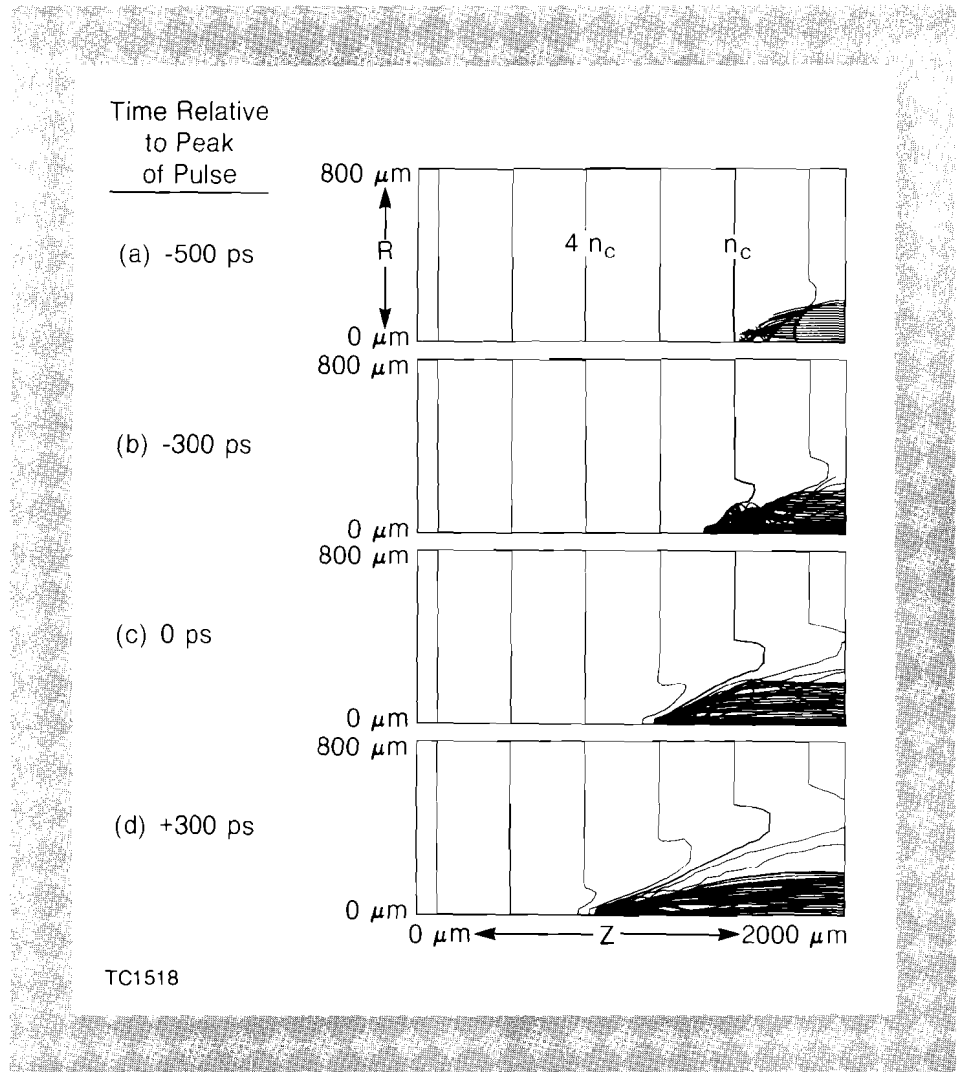


Fig. 18.17
 Results for the standard parameters, but with the laser wavelength changed to 1054 nm. The same electron density profile is assumed, so the critical density is further to the right. A significant fraction of the rays reach the critical density before depositing 90% of their energy, so the reflected rays are also shown. Whole-beam self-focusing is present in (b).

configuration where the laser is obliquely incident on such a preformed plasma, it is reasonable to anticipate that the reflected light would also be directed toward the laser, rather than in the specular direction to the target normal, since the low-density channel is formed by the radial expulsion of plasma from the underdense laser-heated region. The inclusion of the ponderomotive force would probably enhance this effect. (At large angles of incidence, however, the ray trajectories may not be sufficiently bent in the vicinity of the turning point to return along the low-density channel.)

One factor which enhanced the self-focusing in the standard case was the cold background through which the beam propagated, since this plasma was easy to push aside radially. Distinctly different behavior occurs for a hot background, as is shown in Fig. 18.19, where the initial plasma temperature is taken to be 2 keV, comparable to the peak coronal temperature at the peak of the pulse in the standard case. Comparing Fig. 18.19 with Fig. 18.14, it is seen that substantially less lateral motion occurs in Fig. 18.19 because the background plasma is hot. Indented density contours still develop,

Fig. 18.18
 Cumulative distribution of back-reflected light for the calculation of Fig. 18.17 which uses 1054-nm light. Note the strong collimation of the back-reflected light: 80% of this light returns within 12° of the laser beam axis.

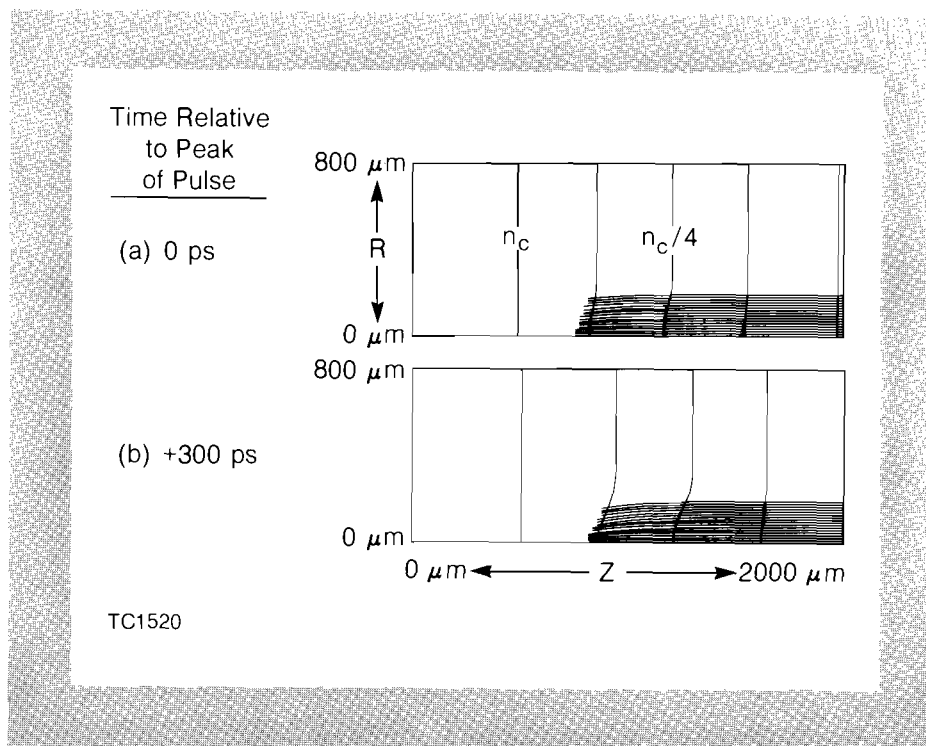
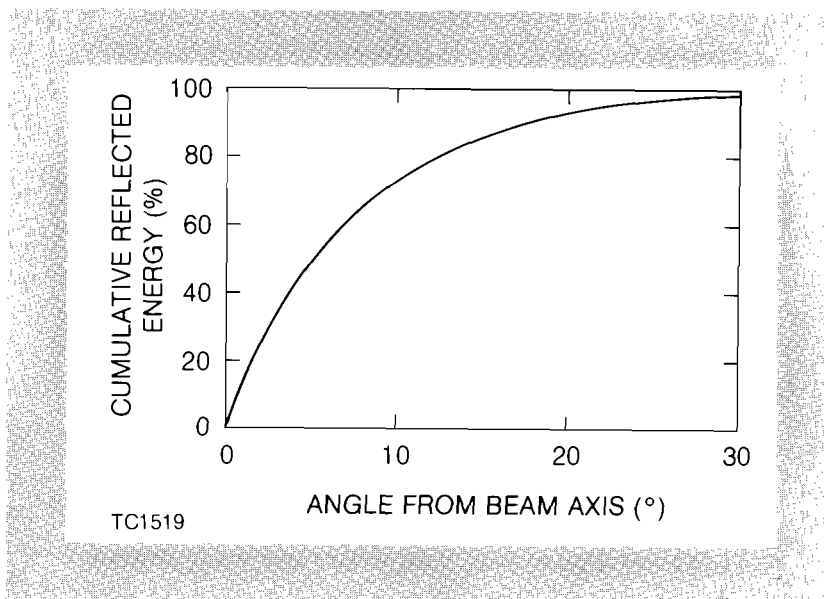


Fig. 18.19
 Results for the standard parameters, but with the background plasma initially at the temperature of 2 keV. Only two times are shown because of the lack of whole-beam self-focusing.

but primarily as a result of greater ablation from the on-axis region which experiences the maximum incident-laser intensity. Self-focusing does not occur, and the depth of penetration of the beam front is considerably reduced relative to the standard case. In the intermediate case of a moderately hot background (1 keV), self-focusing similar to that observed in Fig. 18.14 is seen to occur.

The description of thermal energy transport is probably the biggest uncertainty in the processes modeled in this paper, so the sensitivity

of the results to the flux limiter f has been investigated. This parameter affects the heat flow both parallel and perpendicular to the laser axis. Results obtained using $f = 0.65$ indicate (reassuringly) that the basic self-focusing behavior observed in Fig. 18.14 is not significantly altered.

For laser-fusion applications, an important consideration is the effect of nonuniformity in the incident irradiation. Specifically, if a laser beam contains perturbations (hot spots), will small-scale self-focusing occur, seeded by these perturbations? To examine this question we have performed simulations in which the irradiation profile comprises a radial Gaussian superimposed upon a uniform background. The peak-to-background intensity ratio is varied, but the peak intensity is fixed at the same value as for the standard calculation. It is clearly not feasible, using a code with fewer than three dimensions, to simulate a beam containing more than one hot spot, since each hot spot would probably focus onto its own axis. If we were to impose an off-axis perturbation in our cylindrically symmetric geometry we could model the self-focusing of a ring perturbation, but experimentally it is more probable that such a ring filament would break up into a number of cylindrical filaments.

Results from a series of cases with successively smaller peak-to-background variations are shown in Fig. 18.20, all plotted at the peak of the pulse. In Fig. 18.20(a), the peak-to-background ratio is large (1.5:1), and in comparison with Fig. 18.20(c) it is seen that the hot spot self-focuses much as if the background had not been present. In Figs. 18.20(b)–18.20(d), the extent of self-focusing successively decreases, as expected, with a transition occurring somewhere between a 10% modulation and a 1% modulation. For real experimental situations, this transition point will of course depend on the detailed parameters: for example, a lower transition point would be expected for larger-scale-length plasmas. It is worth noting, though, that irradiation uniformities of better than a few percent should be attainable on multi-beam spherical systems.¹⁰

Conclusions

We have investigated thermal self-focusing in laser-produced plasmas, taking into account effects associated with realistic 2-D plasma hydrodynamics. While it is difficult, if not impossible, to draw quantitative conclusions about thermal self-focusing which will apply to all laser-plasma configurations, it is possible to note some general results. Whole-beam self-focusing has been observed, but only in situations where the beam radius is less than approximately half the plasma scale length. On-axis low-density channels in the underdense plasma have been seen to develop, primarily as a result of radial expansion from a heated region of finite radius, but also from preferential axial expansion from irradiation maxima. Light returning from such channels is expected to be well collimated toward the incident laser.

Experiments involving the interaction of a tightly focused laser beam with a cold, large-scale-length, preformed plasma are expected

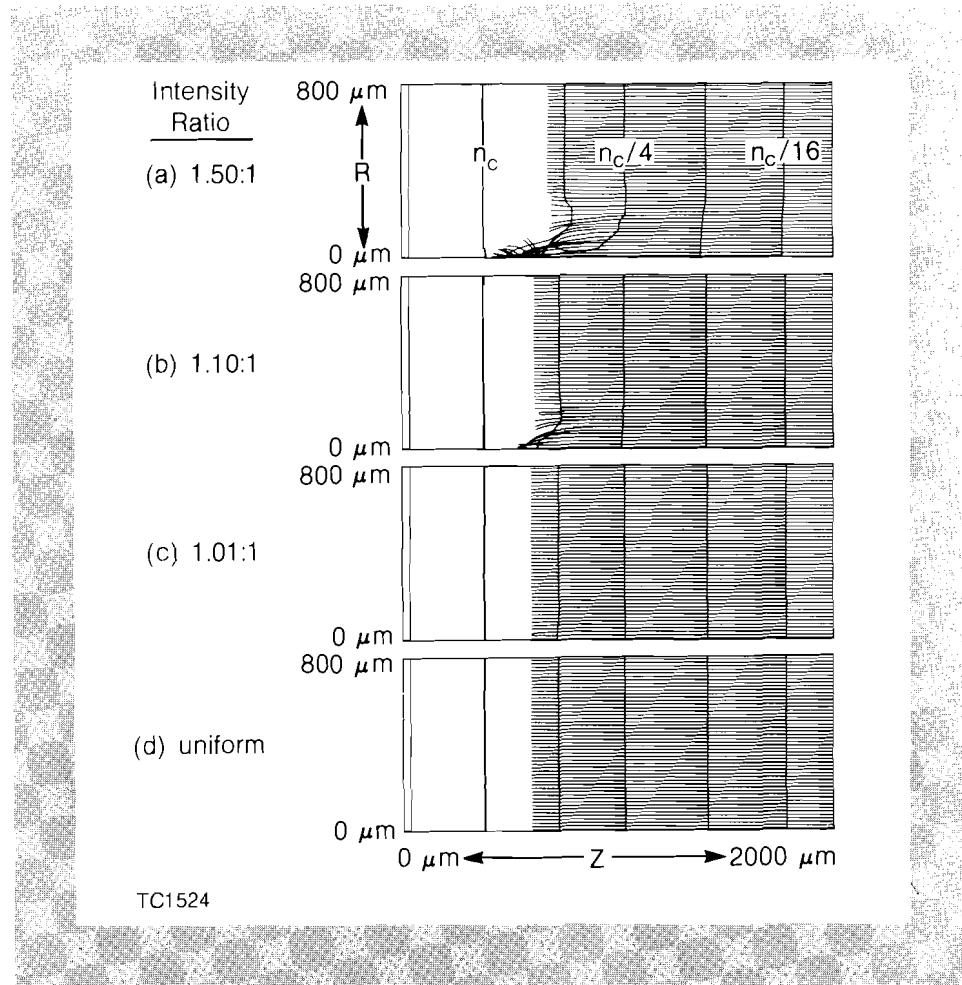


Fig. 18.20

Results for the standard parameters, but with the Gaussian beam superimposed on a uniform background to simulate a hot spot in the incident laser beams. The peak intensity in the Gaussian is held constant at the standard value and the background intensity is changed to generate the intensity ratios noted in the figure. All plots are at the peak of the laser pulse. The transition to whole-beam self-focusing occurs between a 1% and 10% intensity ratio.

to be particularly subject to thermal self-focusing. On the other hand, strong self-focusing is less likely to occur in situations where the background is warm and the laser radiation is uniform with small modulations. It is to be hoped that this latter state of affairs will apply to laser-fusion experiments as longer-scale-length plasmas are encountered. These results are discussed in greater detail in Ref. 11.

ACKNOWLEDGMENT

This work was supported by the U.S. Department of Energy Office of Inertial Fusion under contract number DE-AC08-80DP40124 and by the Laser Fusion Feasibility Project at the Laboratory for Laser Energetics which has the following sponsors: Empire State Electric Energy Research Corporation, General Electric Company, New York State Energy Research and Development Authority, Northeast Utilities Service Company, Southern California Edison Company, The Standard Oil Company, and University of Rochester. Such support does not imply endorsement of the content by any of the above parties.

REFERENCES

1. See for example: A. J. Alcock, C. DeMichelis, V. V. Korobkin, and M. C. Richardson, *Appl. Phys. Lett.* **14**, 145 (1969); H. A. Baldis and P. D. Corkum, *Phys. Rev. Lett.* **45**, 1260 (1980); O. Willi, P. T. Rumsby, and S. Sartang, *IEEE J. Quantum Electron.* **QE-17**, 1909 (1981); C. Joshi, C. E. Clayton, A. Yasuda, and F. F. Chen, *J. Appl. Phys.* **53**, 215 (1982).

2. See for example: S. A. Akhmanov, A. P. Sukhorukov, and R. V. Khokhlov, *Sov. Phys. Usp.* **10**, 609 (1968); F. W. Perkins and E. J. Valeo, *Phys. Rev. Lett.* **32**, 1234 (1974); D. Anderson and M. Bonnedal, *Phys. Fluids* **22**, 105 (1979); D. Subbarao and M. S. Sodha, *J. Appl. Phys.* **50**, 4604 (1979); A. Schmitt and R. S. B. Ong, *J. Appl. Phys.* **54**, 3003 (1983); M. J. Giles, *J. Plasma Phys.* **29**, 325 (1983).
3. M. D. Feit and J. A. Fleck, *Appl. Phys. Lett.* **28**, 121 (1976).
4. R. C. Malone, R. L. McCrory, and R. L. Morse, *Phys. Rev. Lett.* **34**, 721 (1975).
5. R. S. Craxton and R. L. McCrory, Laboratory for Laser Energetics Report No. 108 (1980).
6. LLE Review **16**, 26 (1983).
7. M. Born and E. Wolf, *Principles of Optics*, 5th ed. (Pergamon Press, Oxford, 1975), p. 122.
8. J. H. Gardner *et al.*, Paper M5, 13th Annual Anomalous Absorption Conference, Banff, Alberta, Canada (1983).
9. J. A. Stamper *et al.*, Paper M6, 13th Annual Anomalous Absorption Conference, Banff, Alberta, Canada (1983).
10. S. Skupsky and K. Lee, *J. Appl. Phys.* **54**, 3662 (1983).
11. R. S. Craxton and R. L. McCrory, *J. Appl. Phys.* (to be published).